AD-A140 630   MARS: SUBSURFACE PROPERTIES FROM OBSERVED LONGITUDINAL   1/8
VARIATION OF THE 3..(U) AEROSPACE CORP EL SEGUNDO CA
ELECTRONICS RESEARCH LAB E E EPSTEIN ET AL. 15 MAR 84
UNCLASSIFIED TR-0084(4925-07)-5 SD-TR-84-05   F/G 3/2   NL
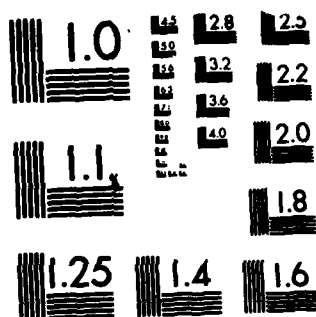
END
DATE
FILMED
*6-84
DTIC

MICROCOPY RESOLUTION TEST CHART

NATIONAL BUREAU OF STANDARDS-1963-A

AD-A140 630

Prepared for

SPACE DIVISION
AIR FORCE SYSTEMS COMMAND
Los Angeles Air Force Station
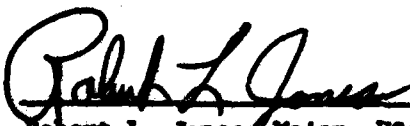P.O. Box 92960, Worldway Postal Center
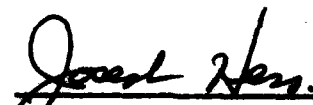Los Angeles, Calif. 90009

DTIC
ELECTE
APR 3 0 1984

A

84 04 30 061

This report was submitted by The Aerospace Corporation, El Segundo, CA 90245, under Contract No. F04701-83-C-0084 with the Space Division, P.O. Box 92960, Worldway Postal Center, Los Angeles, CA 90009. It was reviewed and approved for The Aerospace Corporation by D. H. Phillips, Director, Electronics Research Laboratory. Major Robert L. Jones, SD/YASM, was the project officer for the Mission-Oriented Investigation and Experimentation (MOIE) Program.

This report has been reviewed by the Public Affairs Office (PAS) and is releasable to the National Technical Information Service (NTIS). At NTIS, it will be available to the general public, including foreign nationals.

This technical report has been reviewed and is approved for publication. Publication of this report does not constitute Air Force approval of the report's findings or conclusions. It is published only for the exchange and stimulation of ideas.

Robert L. Jones, Major, USAF
Project Officer

Joseph Hess, GM-15, Director Air Force
Space Technology Center

SECURITY CLASSIFICATION OF THIS PAGE (When Data Entered)

REPORT DOCUMENTATION PAGE		READ INSTRUCTIONS BEFORE COMPLETING FORM
1. REPORT NUMBER SD-TR-84-05	2. GOVT ACCESSION NO. AD-A140 638	3. RECIPIENT'S CATALOG NUMBER
4. TITLE (and Subtitle) MARS: SUBSURFACE PROPERTIES FROM OBSERVED LONGITUDINAL VARIATION OF THE 3.5-MM BRIGHTNESS TEMPERATURE		5. TYPE OF REPORT & PERIOD COVERED
		6. PERFORMING ORG. REPORT NUMBER TR-0084(4925-07)-5
7. AUTHOR(s) Eugene E. Epstein, Bryan H. Andrew, Frank H. Briggs, Bruce M. Jakosky, and Frank D. Palluconi		8. CONTRACT OR GRANT NUMBER(s) F04701-83-C-0084
9. PERFORMING ORGANIZATION NAME AND ADDRESS The Aerospace Corporation El Segundo, Calif. 90245		10. PROGRAM ELEMENT, PROJECT, TASK AREA & WORK UNIT NUMBERS
11. CONTROLLING OFFICE NAME AND ADDRESS Space Division Los Angeles Air Force Station Los Angeles, Calif. 90009		12. REPORT DATE 15 March 1984
		13. NUMBER OF PAGES 29
14. MONITORING AGENCY NAME & ADDRESS(if different from Controlling Office)		15. SECURITY CLASS. (of this report) Unclassified
		15a. DECLASSIFICATION/DOWNGRADING SCHEDULE

16. DISTRIBUTION STATEMENT (of this Report)

Approved for public release; distribution unlimited.

17. DISTRIBUTION STATEMENT (of the abstract entered in Block 20, if different from Report)

18. SUPPLEMENTARY NOTES

19. KEY WORDS (Continue on reverse side if necessary and identify by block number)

Mars, Longitudinal Brightness Temperature Variation
Mars, Millimeter-Wave Observations
Mars, Subsurface Properties

20. ABSTRACT (Continue on reverse side if necessary and identify by block number)

Measurements at 3.5 mm of the disk-average brightness temperature of Mars during the 1978 opposition can be represented by

$$T_B \text{ (Mars, 3.5 mm, Jan/Feb 1978)} = 198_{(+\sigma-1) \pm 1} + 10_{(+\sigma-2) \pm 2} \cos (\text{CML} + 10_{+\sigma-6}^{\pm 6}) \text{ K.} \rightarrow \text{cont}$$

19. KEY WORDS (Continued)

20. ABSTRACT (Continued)

cont →

(The errors cited are from the internal scatter; the estimated absolute calibration uncertainty is 3%.) This longitudinal variation must be taken into account if Mars is to be used as a calibration source at millimeter wavelengths. The total range of the 3.5-mm variation is three to four times larger than both the 2.8-cm and 20-µm variations. This unexpected result can possibly be explained by subsurface scattering from rocks ≲ 1.5-cm radius.

< or approx

PREFACE

CONTENTS

FIGURES

I. INTRODUCTION

Andrew, Harvey and Briggs (1977,1978) measured, and Doherty, Andrew, and Briggs (1979) confirmed, longitudinal variations in Mars' disk-average 2.8-cm radio brightness. These variations indicate variations in the thermal inertia and radiometric albedo in the top decimeter or so of the Martian soil. We have made confirming measurements at 3.5 mm. We use the 3.5-mm, 2.8-cm, and 20-μm data to reach conclusions about subsurface properties.

II. OBSERVATIONS

Observations were made with the NRAO* 11-m telescope at Kitt Peak during three runs in 1978: January 9-12 and 29-31, and February 22-24. The observations on January 9 were obtained during an antenna pointing calibration run and were kindly made available to us by Dr. B. L. Ulich. Inclement weather prevented useful measurements on January 11, 12, and 31. Table 1 describes the Earth-Mars-Sun geometry at the times of the observations. This Mars opposition was quite favorable; Mars' relatively high declination permitted observations through most of the night and Jupiter and Saturn, which served as reference sources, were also at relatively high declinations and were conveniently spaced ~1-1/2 hours in R.A. ahead of and behind Mars, respectively.

A linearly polarized receiving system was used; the double-sideband system temperature at 86.1 GHz (3.5 mm) was ~350 K and the IF bandwidth was 500 MHz. Standard "on-on" beam switching with a 6.6-Hz chopping rate was

---

*The National Radio Astronomy Observatory is operated by Associated Universities, Inc., under contract with the National Science Foundation.
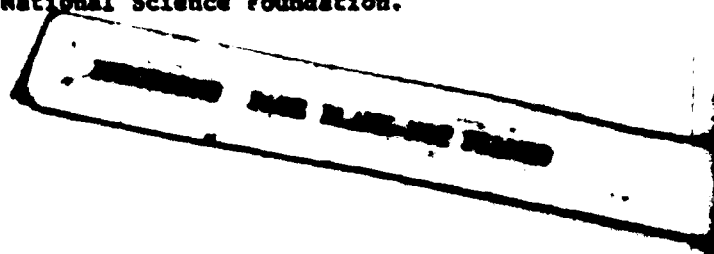
Table 1. Parameters of the Earth-Mars-Sun Geometry at Times of Observations[a]

Parameter	Jan. 9–10	Jan. 29–30	Feb. 22–24
Earth-Mars distance (AU)	0.665 → 0.662	0.664 → 0.668	0.773 → 0.790
Sun-Mars distance (AU)	1.627 → 1.628	1.642 → 1.643	1.656 → 1.656
D_E (deg)	14.0 → 13.8	11.1 → 10.9	9.2 → 9.2
D_S (deg)	12.4 → 12.7	15.6 → 15.8	18.9 → 19.2
A_E + 180 (deg)	219.9 → 219.4	212.6 → 212.1	206.7 → 206.4
$A_S - A_E$ (deg)	−11.4 → −10.2[b]	4.7 → 5.9[b]	21.3 → 22.7[b]
k	0.991	0.996	0.961 → 0.956
1	11.2 → 10.0	6.4 → 8.0	22.8 → 24.1
Central Meridian Longitude (deg)	195 → 312	347 → 138	74 → 246

[a] D_E and D_S are the planetocentric declinations of the Earth and the Sun, respectively, A_E and A_S are the planetocentric right ascensions of the Earth and the Sun; k is the ratio of the illuminated disk to the entire disk; and 1 is the angle between the Earth and the Sun as seen from Mars.

[b] Negative and positive values of $(A_S - A_E)$ correspond to observations with the sub-earth point in the afternoon and morning hemispheres, respectively.

8

employed. The beam throw of 228 arc sec (about 2.6 half-power beamwidths) was in azimuth to eliminate the effects of differential atmospheric emission. An observation was 2 or 3 minutes in duration, depending upon whether it was taken with the conventional "FIVE" or "SEQUENCE" technique. (A SEQUENCE observation consists of a sequence of on-on pairs of readings wherein the telescope is directed so that the planet is measured first in one position of the switched beam, then in the other position. A FIVE observation consists of short SEQUENCE observations in the nominal direction of the planet and at the four cardinal points one-half beamwidth away; it takes more telescope time, but it permits the telescope pointing errors to be derived and compensated for in the data reduction.) A FIVE observation on each planet was always taken first to adjust the telescope pointing for the subsequent SEQUENCE observation.

A FIVE and a SEQUENCE observation of Jupiter and then of Mars were made through the night, until Jupiter was at too low an elevation, at which time Saturn was substituted. Focus checks were made every 2 or 3 hours. Atmospheric attenuation was also determined at similar intervals via "tipping". The zenith optical depth ranged from 0.04 to 0.10 throughout the three observing runs, save for a few hours on January 10 when it was as high as 0.21. The proximity in the sky of the reference sources reduced the deleterious consequences of uncertainties in the atmospheric attenuation corrections.

Absolute calibration was based on the 3.5-mm brightness temperature of Jupiter — 179.4 ± 4.7 K — determined by Ulich et al. (1980). The estimated overall absolute calibration uncertainty is 3%. The changes in the solid angles of the planets over the several weeks of measurements were accounted for in the data reduction. In calculating the source size corrections the antenna pattern was taken to be Gaussian (though not constant — see below)

9

and the planetary disks were assumed to be uniformly bright; Saturn's rings were neglected. However, an observed Jupiter/Saturn signal strength ratio was determined from all the measurements and used in reducing the Mars data obtained when only Saturn was available as a reference. Because the ring inclination angle changed only 1°5 during the course of the measurements and because the 3-mm flux from the Saturn system changes very slowly with inclination angle (Epstein et al., 1984 and Ulich, 1981), we neglected any change in flux from the rings. Although nonthermal emission because of radiation belts produces longitudinal variations of Jupiter's centimeter and decimeter radiation, this nonthermal emission is less than 5% of Jupiter's total emission shortward of 1.5-cm wavelength (Berge and Gulkis, 1976); the rotational variability of the nonthermal emission produces an even smaller percentage variation in the total emission shortward of 1.5 cm. Thus at 3 mm the nonthermal emission component must be quite small. The zonal structure of the visible disk of Jupiter is sufficiently longitudinally symmetric that we do not expect significant longitudinal variations of Jupiter's 3-mm thermal emission. Similar statements apply to Saturn. We know of no evidence to suggest contrary expectations at 3 mm.

The 11-m reflector was not mechanically stable; this fact meant that there was no single relationship between antenna gain and antenna attitude that was valid at all times. Similarly, the antenna pattern, as manifested in the azimuth and elevation half-power beamwidths determined from the FIVE observations, was not constant with time. The beamwidth changes from night to night were not statistically significant, but the changes between the three runs were. These changing beamwidths were taken into account when subsequently reducing the FIVE data. To process the data we did assume that G(z), the relation between gain and zenith angle, was stable for half nights at a time; we determined G(z) from the relevant Jupiter and/or Saturn data.

III. RESULTS

The 131 values of the disk-average 3.5-mm Mars brightness temperatures are plotted against Central Meridian Longitude in Fig. 1. The circled symbols represent data for which Saturn, not Jupiter, served as the reference. No attempt has been made to estimate the uncertainties of the individual values. From working with the data we believe that the major source of scatter is the antenna gain instability; in comparison, uncertainties in intermediate calibration, source size correction, and atmospheric attenuation correction are negligible.

The same data, but grouped into longitude interval bins of equal width, are shown in Fig. 2. Although the scatter is large, the dependence upon CML is clear. There is an unfortunate paucity of data near the indicated peak (CML ~ 320°). A one-harmonic least-squares fit to the unbinned data, with equal weights assumed for all 131 points (it is not possible to assign reliable weights to the points), yields

$$T_B(\text{Mars, 3.5 mm, Jan/Feb 1978}) = 198 + 10 \cos(\text{CML} + 42°) \text{ K}; \quad (1)$$
$$\pm 1 \quad \pm 2 \qquad \qquad \pm 12$$

the standard deviation of the residuals is 8.6 K. The errors cited represent the internal scatter only; the estimated absolute calibration uncertainty is 3%. [We explicitly denote the epoch of observations because Mars' brightness temperature is a function of epoch and observational aspect (Cuzzi and Muhleman, 1972).] A two-harmonic fit yields
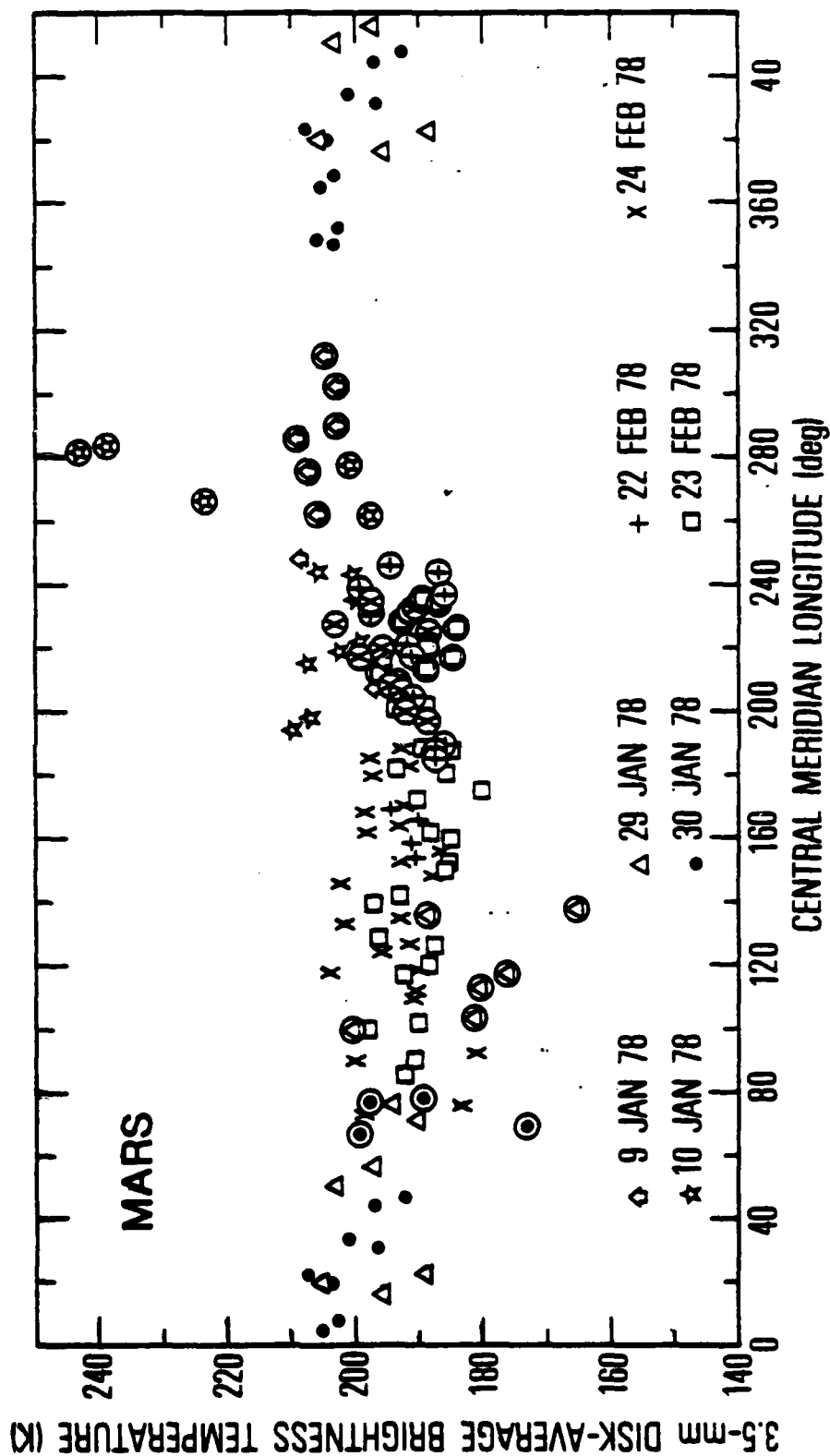
Fig. 1. Disk-Average 3.5-mm Martian Brightness Temperatures vs. Central Meridian Longitude. The circled symbols represent data for which Saturn served as the reference; Jupiter served as the reference for all other data.
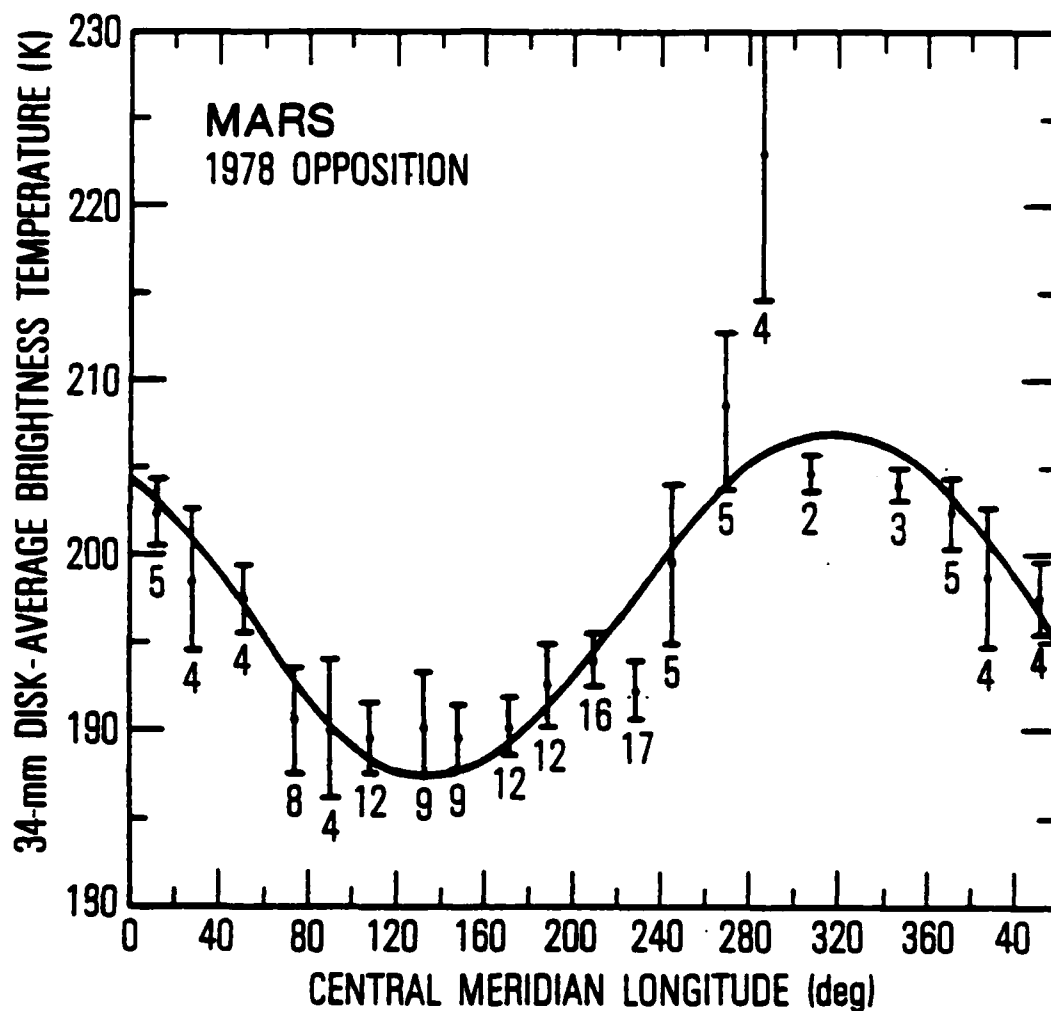
Fig. 2. Disk Average 3.5-mm Martian Brightness Temperatures vs. Central Meridian Longitude, Bin Averages. The statistical standard errors of the bin averages are indicated. The numerals represent the number of data points in the bin average. The curve shown is the unweighted least-squares one-harmonic best fit to the 131 individual data points: T_B(Mars, 3.5 mm) = 198 + 10 cos(CML + 42°) K.

$$T_B(\text{Mars, 3.5 mm, Jan/Feb 1978}) =$$

$$198 + 12 \cos(CML + 48°) - 4 \cos(2 \; CML - 76°) \; K; \qquad (2)$$
$$\pm 1 \quad \pm 2 \qquad\qquad \pm 12 \quad \pm 3 \qquad\qquad\qquad \pm 20$$

because the standard deviation of the residuals reduces only to 8.3 K, and because the amplitude of the second harmonic term is not statistically significant, this two-harmonic fit is not meaningful. The one-harmonic fit is shown in Fig. 2.

These results indicate that if Mars is to be used as a calibration source at 3 mm, the CML at the time of observation must be taken into account if precision to better than ~ ±5% is sought.

Data from the early January and February runs overlap in the interval 195° ≤ CML ≤ 246°; in this interval the average of the February data is 5.5 ± 0.8% lower than the average of the early January data. Data from the late January and February runs overlap in the interval 72° ≤ CML ≤ 140°; the February average is 4.3 ± 2.0% higher than the late January average. We attribute these discrepancies to the combination of three effects: a) the sub-earth local time of day changed by about 2 hours over the three runs, i.e., $(A_S - A_E)$ changed by ~ 33°; b) the polar cap was rapidly shrinking; and c) the planetocentric declination of the Sun (D_S) increased ~ 7° as the declination of the Earth (D_E) decreased by ~ 5°. [Assuming that the 3-mm brightness temperatures scale with heliocentric distance as $r^{-1/4}$ (Doherty et al., 1979) means that the brightness temperature decreased only 0.4% during the course of our observations.] Effect (a) means that the observed sub-Earth points in early January and February corresponded, respectively, to early afternoon and to late morning on Mars. Hence we expect the February (late morning) average to be lower than the early January (afternoon) average.

14

Similarly, we expect the February average to be lower than the late January average, but by not as much. However, the decline in the disk-average brightness temperature as the phase angle changes is likely to be at least somewhat offset as the cold polar cap shrinks and the Sun's declination increases. Predicting numerical values for the combination of these effects would require extensive calculations, and the values would be model dependent. Instead, we made an empirical adjustment for these effects by simply scaling, separately, all of the early January data and all of the late January data to bring into agreement the respective average brightness temperatures with the February averages in the respective longitude intervals of overlap.

The results after these adjustments are shown in Figs. 3 and 4. The overall scatter is visibly reduced. The one-harmonic fit to the unbinned data (shown in Fig. 4) is

$$T_B(\text{Mars, 3.5-mm adjusted data, Jan/Feb 1978}) = 198 + 10 \cos(\text{CML} + 10°) \text{ K; (3)}$$
$$\pm 1 \quad \pm 1 \qquad\qquad \pm 6$$

the standard deviation of the residuals is 7.4 K. A two-harmonic fit yields

$$T_B(\text{Mars, 3.5-mm adjusted data, Jan/Feb 1978}) =$$
$$198 + 11 \cos(\text{CML} + 12°) + 2 \cos(2 \text{ CML} + 29°) \text{ K;} \qquad (4)$$
$$\pm 1 \quad \pm 2 \qquad\qquad \pm 7 \quad \pm 2 \qquad\qquad \pm 35$$

the standard devi   n of the residuals is 7.2 K. Again, the two-harmonic fit is not meaning u   one-harmonic fit to the adjusted data is essentially the same as Eq.   s   >r a 30° phase shift.

For comparison, Doherty et al. (1979) obtained the following two-harmonic fit to their 1978 opposition 2.8-cm data:

15

Fig. 3. Disk-Average 3.5-mm Martian Brightness Temperatures vs. Central Meridian Longitude, Adjusted Data. Same as Fig. 1 except for adjusted data (see Section III).
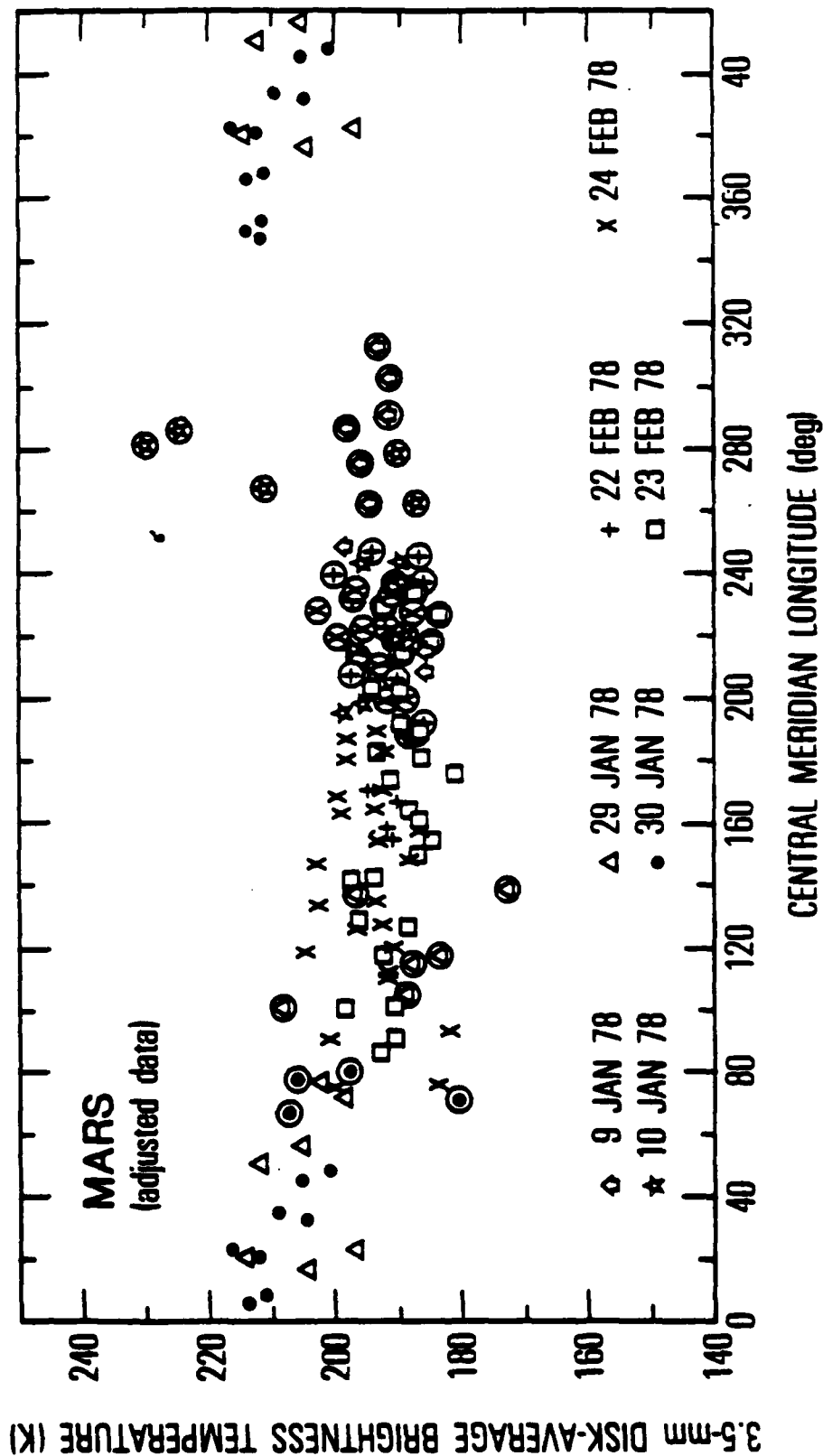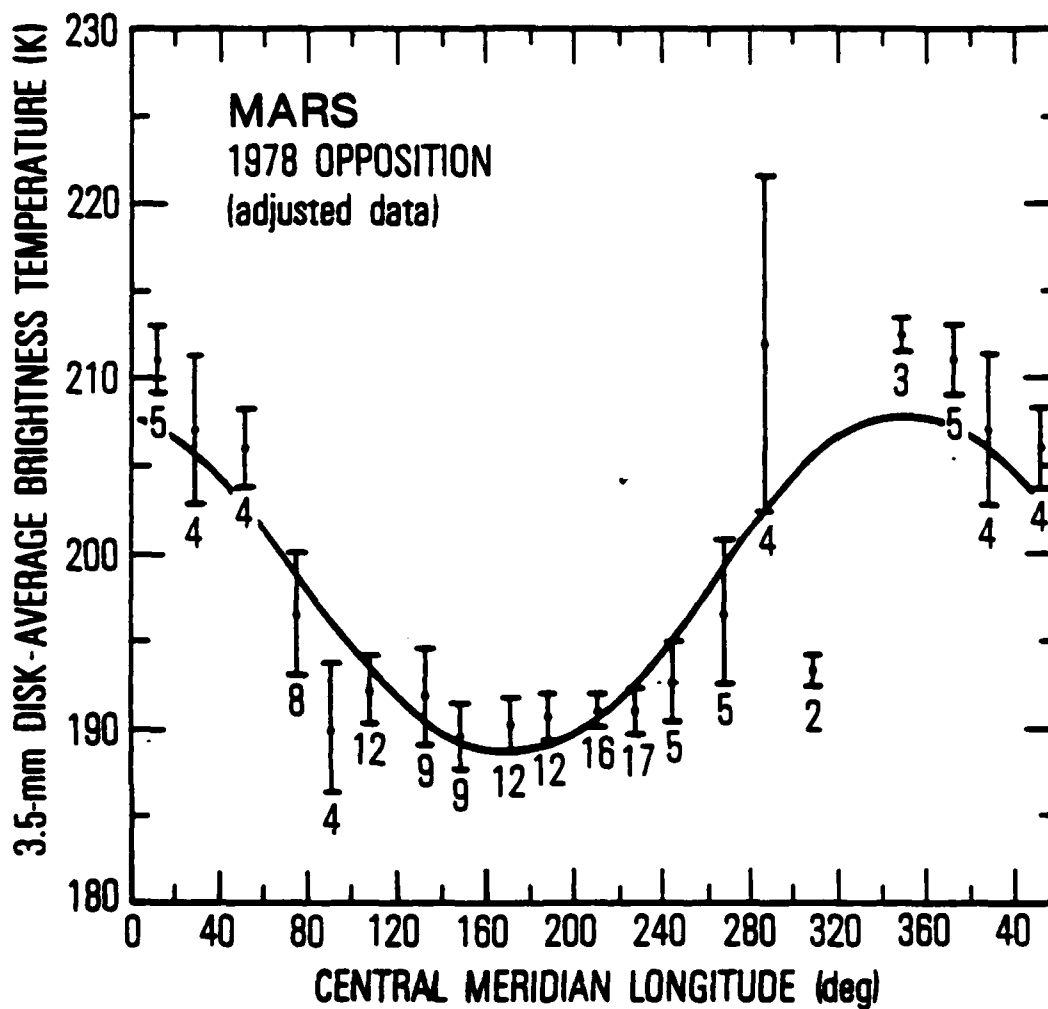
16

Fig. 4. Disk-Average 3.5-mm Martian Brightness Temperatures vs. Central Meridian Longitude, Adjusted Data, Bin Averages. Data same as Fig. 2 except for adjusted data (see Section III). The curve shown is the unweighted least-squares one-harmonic best fit to the 131 individual adjusted data points: T_B(Mars, 3.5-mm adjusted data) = 198 + 10 cos(CML + 10°) K.

T_B(Mars, 2.8 cm, Jan/Feb 1978) =

$$191.5 + 1.1 \cos(CML - 37°) + 1.6 \cos(2\ CML - 134°)\ K. \qquad (5)$$
$$\pm 0.4 \quad \pm 0.8 \qquad\qquad \pm 38 \quad \pm 0.8 \qquad\qquad\qquad \pm 18$$

[Doherty et al. corrected their data to a mean heliocentric distance of 1.524 AU using an $r^{-1/4}$ scaling factor; we have removed this correction from Eq. (5). The 3.5-mm and 2.8-cm data were taken at almost identical heliocentric distances.] The higher of the two 2.8-cm peaks occurs at CML ~ 60°, i.e., ~ 70° after the 3.5-mm peak; however, the 3.5-mm trough and the deeper 2.8-cm minimum both occur at CML ~ 160° (see Fig. 5). The estimated absolute calibration uncertainties in the 3.5-mm and 2.8-cm data are 3% (6 K) and 2% (4K) on the constant terms in Eqs. (1) and (3), respectively; therefore the difference between the mean levels of the 3.5-mm and 2.8-cm data is not significant. There is a difference, however, in the amplitudes of the curves, which is discussed below.

IV. DISCUSSION

The Mars rotational curve at 3.5 mm can be compared with those obtained at other radio wavelengths and in the thermal infrared (Fig. 5). The Viking Orbiter 1 20-µm observations made at the same opposition (Christensen et al., 1978; P. R. Christensen, personal communication, 1981) show a total variation of the disk-average brightness temperature with longitude of ~ 7 K and are represented by

T_B (Mars, 20 µm, Dec 1977/Feb 1978) =
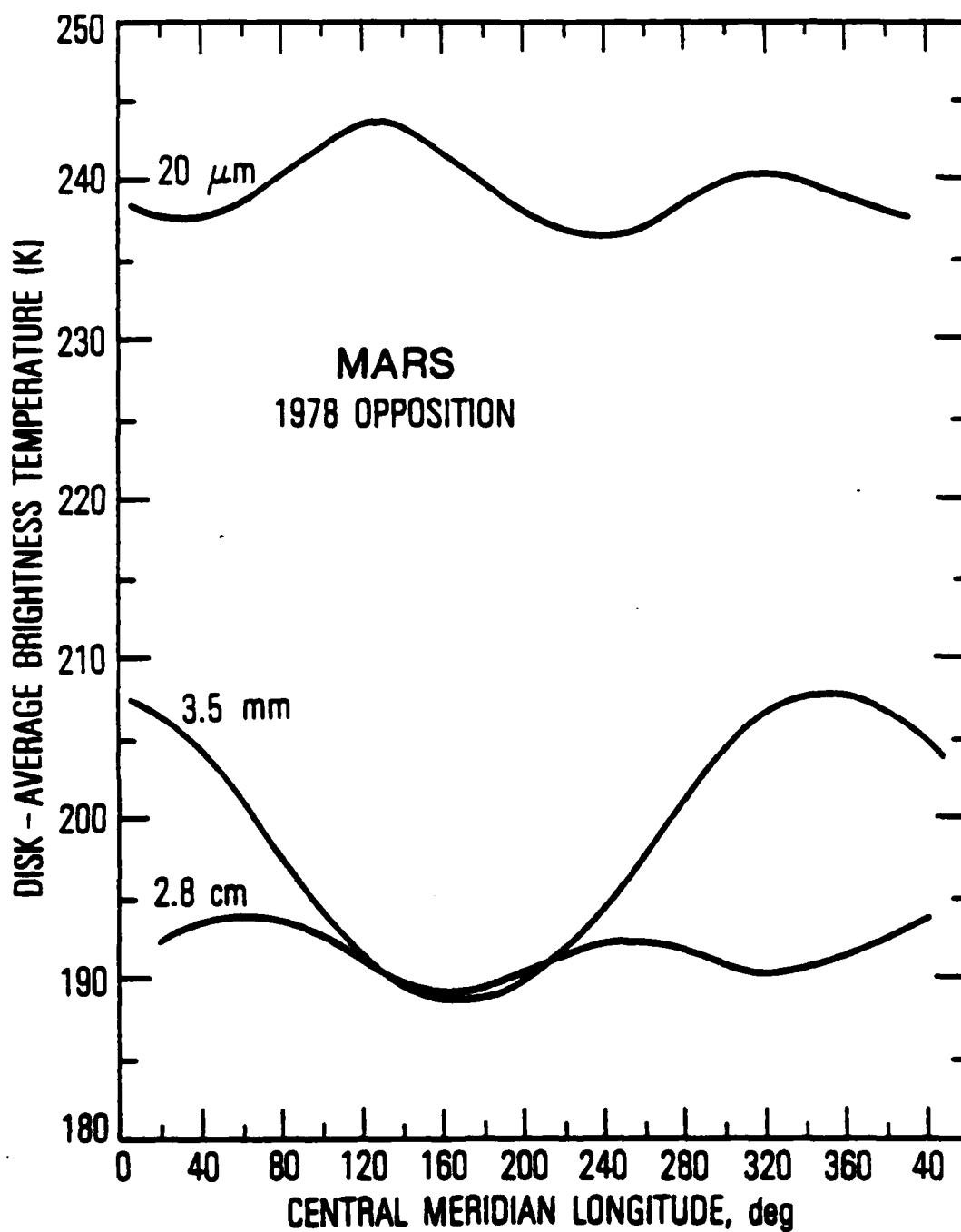
Fig. 5. Best Fits to 1978 Opposition Martian Disk-Average
Brightness Temperatures at 20 μm, 3.5 mm, and
2.8 cm vs. Central Meridian Longitude. The 20-μm
result [Eq. (6)] is from Christensen et al. (1978),
the 3.5-mm curve [Eq. (3)] is the same as in Fig. 4,
and the 2.8-cm result [Eq. (5)] is from Doherty
et al. (1979).

19

$$239.4 - 1.7 \cos(CML - 67°) - 2.4 \cos(2CML - 90°) \text{ K;}$$
$$\pm 0.1 \quad \pm 0.1 \qquad\qquad \pm 6 \quad \pm 0.2 \qquad\qquad\qquad \pm 3 \qquad\qquad (6)$$

the standard deviation of the residuals is 0.6 K. These data refer to a sub-spacecraft local time of ~ 1/4 hour before noon.

The variations correspond to predominantly viewing regions of high thermal inertia and low albedo or regions of low inertia and high albedo, with the low-inertia regions coinciding with the greatest temperatures. Low thermal inertia regions are characterized by a large amplitude, shallowly penetrating temperature wave, whereas high thermal inertia regions experience a lower amplitude but more deeply penetrating temperature wave. This effect results from the control of the surface thermal inertia (defined as $\sqrt{K\rho C}$, where K is the thermal conductivity, ρ is the density, and C is the specific heat of the surface material) on the surface temperature, such that a region of low thermal inertia will have higher temperatures near noon than a region of high thermal inertia (e.g., Kieffer et al., 1977). Because Earth-based observations are generally of the day side of Mars, these near-noon temperatures are emphasized (Christensen et al., 1978). There is considerable thermal diversity on Mars (Palluconi and Kieffer, 1981), such that regions of low or high inertia are alternately visible as the planet rotates, producing a significant rotational variation of brightness temperature.

The rotational curve is quite different at radio wavelengths. Measurements at 2.8 cm (Andrew et al., 1977, 1978; Doherty et al., 1979), which show a peak-to-peak variation in disk-average temperature with amplitude of about 5 K, compared to about 20 K at 3.5 mm, indicate that the high temperatures correspond to preferential viewing of the regions of high inertia (Jakosky and Muhleman, 1980). This difference can be understood in terms of the subsurface temperatures and the penetration depth of the 2.8-cm radiation. The e-folding

20

electrical skin depth is typically ~10λ, or ~30 cm here (see Campbell and Ulrichs, 1969; Muhleman, 1972; or Cuzzi and Muhleman, 1972), such that the bulk of the observed energy comes from beneath the diurnal thermal skin depth of 5-10 cm. Therefore, the observations are most sensitive to the temperature at depth; because high-inertia regions have a greater average daily temperature than low-inertia regions, due to the nonlinearity of the Planck function and the generally lower albedo in high-inertia regions, the trend is to see higher disk-average temperatures when viewing the high-inertia regions (Jakosky and Muhleman, 1980). The dominant effect is the Planck function nonlinearity. To maintain radiative equilibrium over an entire day, there must be a balance between the lower emission rates during the day (because of lower daytime temperatures of high-inertia regions) and the higher emission rates at night (caused by higher nighttime temperatures). Because of the nonlinearity, the increase in the nighttime temperature must be greater than the decrease in daytime temperatures to produce the same magnitude of effect on the emission rates (Jakosky and Muhleman, 1980).

It is because the infrared and radio observations are so different that the 3.5-mm measurements reported here are of interest (in addition to obtaining data pertaining to Mars as a millimeter-wave calibration source). At some wavelength between 20 μm and 2.8 cm the behavior must change from that seen at 2.8 cm, with high-inertia regions having higher disk-average temperatures, to that seen at 20 μm, with low-inertia regions having higher disk-average temperatures. That is, there is likely a wavelength where the disk-average brightness temperature does not vary significantly with longitude. The wavelength at which this occurs, as well as the suite of rotational curves at nearby wavelengths, will yield information relevant to the physical nature of the surface of Mars, as will be discussed below.

Although properly calculating the rotational curve for Mars at radio and infrared wavelengths is a formidable task, even for the simplest cases, some simple calculations can be done to identify the wavelength at which the cross-over in behavior may occur. Figure 6 shows contour plots of the modelled noontime nadir-viewing microwave brightness temperature as a function of the thermal inertia and the radiation penetration e-folding skin depth for several sets of assumptions regarding emissivities at radio and infrared wavelengths. These results were obtained by calculating the diurnal surface temperature variation for a given set of thermal properties, extrapolating the temperature variation to depth, and integrating the emission of energy over depth at local noon, using a technique similar to that described by Muhleman (1972) and Jakosky and Muhleman (1980). Each calculation is done assuming a homogeneous surface, with properties uniform with depth; thermal inertia and surface albedo were taken to be related as described by Kieffer et al. (1977). In Fig. 6a, the infrared emissivity e_{IR} was taken to be 1.0, and the microwave emissivity e_M was a constant; in Fig. 6b, e_{IR} was taken to be correlated with albedo, and hence inversely with inertia, as per the results of Christensen (1982); in Fig. 6c, e_{IR} correlates with albedo and e_M was taken to be related to inertia as indicated by the correlation of radar cross-section and inertia (Jakosky and Muhleman, 1981). These assumptions represent the range of possible variations of surface properties, exclusive of roughness and scattering effects, which are discussed further below.

The penetration depth at which the noontime temperature varies the least with thermal inertia (and hence with longitude as the planet rotates) is that for which the rotational curve would be expected to show the least variation of temperature with longitude. From Fig. 6, this situation occurs for a penetration depth of between 0.4 and 1.6 cm, depending on the assumptions

22
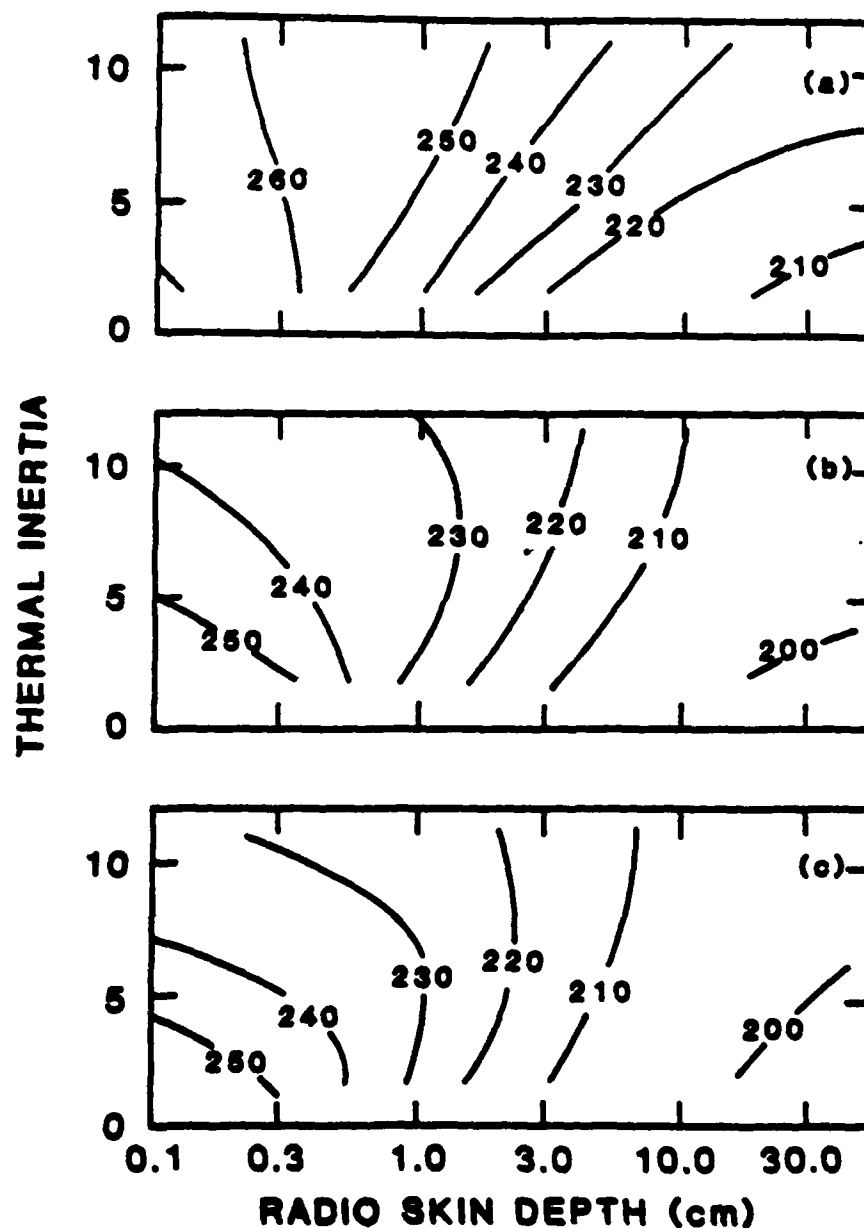
Fig. 6. Noontime Nadir-Viewing Microwave Brightness Temperature
as a Function of the Surface Thermal Inertia and the
Radio Skin Depth (in cm). (a) Assuming constant infrared and
microwave emissivity. (b) Assuming infrared emissivity
varies with albedo (and, hence, with inertia).
(c) Same as (b), but also allowing microwave emissivity
to be correlated with thermal inertia. See text for details.

made. In the absence of roughness and scattering effects, the wave-length λ and the penetration skin depth δ are related by $\delta = n\lambda$, where n is between about 5 and 20 for particulate surfaces (Campbell and Ulrichs, 1969). Thus the cross-over point should occur for an observing wavelength between about 0.2 and 3.2 mm. For material properties like that of the Moon (n $\approx$ 15; Muhleman, 1972; Gary and Keihm, 1978), the corresponding wave-length range would be 0.3 to 1.1 mm.

Surface roughness may affect these results in two ways. First, centi-meter-sized and larger surface rocks may perturb the situation. If rocks are present in large enough numbers to affect the bulk surface thermal inertia, as indicated by the radar/thermal analysis of Jakosky and Muhleman (1981), then the above calculations may not be adequate; they are sufficient if the rock abundance were to not vary significantly from place to place and if the ther-mal inertia were determined by the properties of the fine component of the surface, as suggested by Christensen (1982). In the former case, the observed flux will be the sum of that from the fine material and that from the rock, weighted by the fraction of the surface covered by each. The penetration depth for which the rock and fine components of the surface have the same brightness temperatures at noon corresponds to the wavelength for which rota-tional variation of disk-average temperature will be small or negligible; for flat rocks larger than the thermal skin depth, under assumptions equivalent to those in Fig. 6a, this equality occurs for a penetration skin depth of about 1.5 cm, within the range discussed above.

Second, surface roughness on the scale of the observing wavelength or subsurface scattering will modify the discussion of skin depths. In the surface roughness case, observed energy will have been scattered at the sur-face, effectively having been emitted from shallower regions than expected

based purely on the material's electrical properties. The effective value for n will then be smaller than the range of 5 to 20 discussed above. There is no direct information on the structure of the Mars surface on the scale of interest here, about 0.2 to 3 mm, except at the Viking landing sites where no significant roughness on these scales is seen (e.g., Mutch et al., 1976 a,b). Scattering by subsurface rocks will have the same effect, such that emission will be from shallower regions and the effective value for n will be smaller. Keihm (1982) calculates for the lunar case that reasonable subsurface rock distributions can decrease n by more than a factor of two over the homogeneous case. Because of the subsurface temperature structure near noon, the effect of decreasing n is to increase the brightness temperature. This point is discussed further below.

In light of the above discussion, the cross-over from the behavior of the rotational curve seen at radio wavelengths to that seen in the infrared should occur at a wavelength within the range of about 0.2 to 3 mm, assuming a homogeneous surface and subsurface. The wavelength at which it occurs will yield information on the Mars electrical properties and roughness-related emissivity effects. The 3.5-mm observations presented here show behavior more like that seen at 2.8 cm rather than that seen at 20 μm. The lower disk-average temperatures coincide with the low-inertia regions near 120° longitude (the Tharsis region), while the higher temperatures generally correspond to the high-inertia regions over most of the remaining longitudes. The uncertainty in the measurements may account for not being able to identify in the 3.5-mm data all of the longitudinal structure seen in the thermal inertia map of Palluconi and Kieffer (1981).

The difference between the absolute levels of the 3.5-mm and 2.8-cm curves is not statistically significant (see Sec. III). The similarity in

25

levels results from the fact that both wavelengths are sensitive to emission from depths comparable to or greater than the thermal diurnal skin depth (on average, about 4 to 6 cm; Kieffer, 1976), and again indicates that 3.5 mm is longward of the cross-over point.

The difference between the amplitudes of the 3.5-mm and the 2.8-cm curves is most important. For a homogeneous subsurface one would expect the amplitude of the rotational curve to generally decrease with decreasing radio wavelength until the cross-over point is reached, after which the amplitude would increase (but out of phase with the radio curve) with further decreasing wavelength. That the amplitude increases in going from 2.8 cm to 3.5 mm indicates that subsurface scattering may be important. That the high 3.5-mm brightness temperatures generally coincide with the high temperatures of the 2.8-cm curve and with the high-inertia regions indicates that the subsurface scatterers are located in the high-interia regions. To effectively scatter the 3.5-mm but not the 2.8-cm waves, the scattering efficiency must be larger at the shorter wavelength; the scattering results presented by Hansen and Travis (1974) indicate this to be the case if the scatterers are smaller than about 1.5-cm radius. The distribution of surface rocks seen at the Viking lander sites, however, peaks near 5 - 10 cm radius (e.g., Mutch et al., 1976a, b; 1977), and has a paucity of centimeter-sized rocks (Mutch et al., 1977). It is conceivable that centimeter-sized roughness elements on the surfaces of the larger rocks are responsible for the scattering, or that the lander sites are not typical of the entire planet; that this latter idea is plausible is suggested by the differences between the Viking Lander 1 region and other locations in thermal and radar properties, both of which are also related to rock abundance (Jakosky and Muhleman, 1981).

The requirement that the high-inertia regions contain additional scatterers is consistent with the hypothesis that the thermal inertia of the surface is largely controlled by the abundance of surface rocks (Jakosky and Muhleman, 1981), but inconsistent with the relatively constant rock abundances inferred by Christensen (1982). Christensen's inference is model-dependent, however, in that the results obtained would differ, depending on the size of rock assumed to be present; the correlation of rock abundance with inertia that he presents may, in fact, indicate this to be the case.

V. SUMMARY AND CONCLUSIONS

The extensive 3.5-mm measurements reported here show a variation in Mars' brightness temperature with Central Meridian Longitude that is generally in phase with the variation at 2.8 cm, and opposite in sign from the variations at 20 μm. This phase result is not unexpected because 3.5 mm is longer than the wavelength at which the phase behavior is expected to change.

Unexpected, however, is the result that the 3.5-mm rotation curve amplitude is larger than the amplitudes at both 20 μm and 2.8 cm. This result can be explained by subsurface scattering from rocks smaller than 1.5-cm radius. A correlation of subsurface scatterers with the location of the high-thermal inertia regions would be consistent with the hypothesis that, predominantly, the rock abundance determines the thermal inertia.

Because the amplitude of the 3.5-mm rotation curve is larger than expected, and because the 3.5-mm measurements were hindered by instrumental difficulties, further millimeter-wave measurements are important — at ~ 3 mm to confirm the present results and at $\leq$ 1 mm to better understand the nature of Mars' subsurface. Additionally, more detailed radiative transfer models

27

are justified to better account quantitatively for the present behavior and thereby constrain the scattering models and to permit adjustment for the seasonal effects discussed in Section III. Such observations and models are now being planned.

REFERENCES

Andrew, B. H., Harvey, G. A., and Briggs, F. H. (1977). Rotational variations in the radio brightness of Mars. Astrophys. J. (Letters) 213, L131-L34.

Andrew, B. H., Harvey, G. A., and Briggs, F. H. (1978). Rotational variations in the radio brightness of Mars — erratum. Astrophys. J. (Letters) 220, L61.

Berge, G. L., and Gulkis, S. (1976). Earth-based radio observations of Jupiter: millimeter to meter wavelengths. In Jupiter (T. Gehrels, ed.), 621-692. University of Arizona Press, Tucson.

Campbell, M. J. and Ulrichs, J. (1969). Electrical properties of rocks and their significance for lunar radar observations. J. Geophys. Res. 74, 5867-5881.

Christensen, P. R. (1982). Martian dust mantling and surface composition: interpretation of thermophysical properties. J. Geophys. Res. 87, 9985-9998.

Christensen, P. R., Kieffer, H. H., and Palluconi, F. D. (1978). Mars as an infrared calibration standard: incorporation of Viking IRTM results. Bull. Am. Astron. Soc. 10, 572-573.

Cuzzi, J. N. and Muhleman, D. O. (1972). The microwave spectrum and nature of the subsurface of Mars. Icarus 17, 548-560.

Doherty, L. H., Andrew, B. H., and Briggs, F. H. (1979). Confirmation of the longitudinal dependence of the radio brightness of Mars. Astrophys. J. (Letters) 233, L165-L168.

Epstein, E. E., Janssen, M. A., and Cuzzi, J. N. (1984). Saturn's rings: 3-mm low-inclination observations and derived properties. Submitted to Icarus.

Gary, B. L. and Keihm, S. J. (1978). Interpretation of ground-based microwave measurements of the moon using a detailed regolith properties model. Proc. Lunar Planet. Sci. Conf. 9th, 2885-2900.

Hansen, J. E. and Travis, L. D. (1974). Light scattering in planetary atmospheres. Space Sci. Rev. 16, 527-610.

Jakosky, B. M. and Muhleman, D. O. (1980). The longitudinal variation of the thermal inertia and of the 2.8 centimeter brightness temperature of Mars. Astrophys. J. 239, 403-409.

Jakosky, B. M. and Muhleman, D. O. (1981). A comparison of the thermal and radar characteristics of Mars. Icarus 45, 25-38.

Keihm, S. J. (1982). Effects of subsurface volume scattering on the lunar microwave brightness temperature spectrum. Icarus 52, 570-584.

Kieffer, H. H., Martin, T. Z., Peterfreund, A. R., Jakosky, B. M., Miner, E. D., and Palluconi, F. D. (1977). Thermal and albedo mapping of Mars during the Viking primary mission. J. Geophys. Res. 82, 4249-4291.

Kieffer, R. H. (1976). Soil and surface temperatures at the Viking landing sites. Science 194, 1344-1346.

Muhleman, D. O. (1972). Microwave emission from the Moon, in Thermal Characteristics of the Moon (J. W. Lucas, ed.), MIT Press, Cambridge, 51-81.

Mutch, T. A., Binder, A. B., Huck, F. O., Levinthal, E. C., Liebes, Jr., S., Morris, E. C., Patterson, W. R., Pollack, J. B., Sagan, C., and Taylor, G. R. (1976a). The surface of Mars: the view from the Viking 1 Lander. Science 193, 791-801.

Mutch, T. A., Grenander, S. U., Jones, K. L., Patterson, W. R., Arvidson, R. E., Guinness, E. A., Avrin, P., Carlston, C. E., Binder, A. B., Sagan, C., Dunham, E. W., Fox, P. L., Pieri, D. C., Huck, F. O., Rowland, C. W., Taylor, G. R., Wall, S. D., Kahn, R., Levinthal, E. C., Liebes, Jr., S., Tucker, R. B., Morris, E. C., Pollack, J. B., Saunders, R. S., and Wolf, M. R. (1976b). The surface of Mars: the view from the Viking 2 Lander. Science 194, 1277-1283.

Mutch, T. A., Arvidson, R. E., Binder, A. B., Guinness, E. A., and Morris, E. C. (1977). The geology of the Viking Lander 2 site. J. Geophys. Res. 82, 4452-4467.

Palluconi, F. D. and Kieffer, H. H. (1981). Thermal inertia mapping of Mars from 60°S to 60°N. Icarus 45, 415-426.

Ulich, B. L. (1981). Millimeter-wavelength continuum calibration sources. Astron. J. 86, 1619-1626.

Ulich, B. L., Davis, J. H., Rhodes, P. J., and Hollis, J. M. (1980). Absolute brightness temperature measurements at 3.5 mm wavelength. IEEE Trans. Antennas Propagat. AP-28, 367-376.

sources.

Absolute
EE Trans.

END

DATE
FILMED

6-8

DTIC